Ann Microbiol (2014) 64:1055–1063
DOI 10.1007/s13213-013-0744-4

ORIGINAL ARTICLE

Biogenic synthesis of floral-shaped gold nanoparticles using a novel strain, *Talaromyces flavus*

Eepsita Priyadarshini · Nilotpala Pradhan · Lala Behari Sukla · Prasanna Kumar Panda · Barada Kanta Mishra

Received: 21 June 2013 / Accepted: 22 October 2013 / Published online: 19 November 2013

Abstract A biogenic route was adopted towards the synthesis of gold nanoparticles using the extract of a novel strain, *Talaromyces flavus*. Reduction of chloroauric acid by the fungal extract resulted in the production of gold nanoparticle, which was further confirmed by the concordant results obtained from UV–visible spectroscopy, energy dispersive spectroscopy (EDS), and dynamic light scattering (DLS) analysis. Morphology and the crystal nature of the synthesized nanoparticles were characterized using transmission electron microscopy (TEM), X-ray diffraction (XRD) and selected area electron diffraction (SAED). A direct correlation was observed between nanoparticle formation and the concentration of reducing agent present in the fungal extract. The time-dependent kinetic study revealed that the bioreduction process follows an autocatalytic reaction. Crystalline, irregular, and mostly flower-shaped gold nanoparticles with a mean hydrodynamic radius of 38.54±10.34 nm were obtained. pH played a significant role on production of mono-dispersed nanoparticle. FTIR analysis partially deciphered the involvement of $–NH_2$, −SH, and –CO groups as the probable molecules in the bio-reduction and stabilization process. Compared to the conventional methods, a time-resolved, green, and economically viable method for floral-shaped nanoparticle synthesis was developed.

Electronic supplementary material The online version of this article (doi:10.1007/s13213-013-0744-4) contains supplementary material, which is available to authorized users.

E. Priyadarshini (✉) · N. Pradhan
Academy of Scientific and Innovative Research, CSIR-Institute of Minerals and Materials Technology, Bhubaneswar 751013, India
e-mail: lisa.eepsita@gmail.com

N. Pradhan · L. B. Sukla · P. K. Panda
Bioresources Engineering Department, CSIR-Institute of Minerals and Materials Technology, Bhubaneswar 751013, India

B. K. Mishra
CSIR- Institute of Minerals and Materials Technology, Bhubaneswar 751013, India

Keywords Biogenic synthesis · Gold nanoparticle · *Talaromyces flavus* · Extracellular · Nanobiotechnology

Introduction

The last decade has been witnessing a fascinating area of research termed nanotechnology: "the synthesis and fabrication of nanomaterials and their applicability" (Eustis and El-Sayed 2006). The European Union Commission defines nanoparticles as "particles having one or more dimensions in the size range of 1−100 nm" and nanomaterials as "natural, incidental or manufactured material containing particles, in an unbound state or as an aggregate or an agglomerate and where, for 50 % or more of the particles in the number size distribution, one or more external dimensions is in the size range 1–100 nm." The increasing application of nanomaterials concomitant with their growing demand has led to the development of a plethora of routes for their synthesis and size modification. Among the noble metals (silver, gold, and platinum), gold has been of paramount importance since ancient times. However, gold nanoparticles (GNP) in comparison to bulk gold have attracted specific attention because of their interesting optical and catalytic properties (Sardar et al. 2009; Eustis and El-Sayed 2006).

GNP have found application in diverse fields like optics (Hong and Hall 2012), electronics (Schmid and Simon 2005), electrochemistry (Huang et al. 2005), catalysis (Stratakis and Garcia 2012), sensing and detection agents (Scampicchio et al. 2006), and in biomedical spheres (Dykman and Khlebtsov 2012) because of their stability, resistance to oxidation, and biocompatibility. Recently, GNP are being widely used for catalysis and SERS studies, which demand the use of complex multi-shaped nanostructures like star-shape, urchin-like, and floral-shaped (Boca et al. 2011; Nehl et al. 2006). Such a shape enhances the total surface area as well as show an enhanced Raman scattering effect. Floral-shaped

GNP in comparison with spherical GNP is known to exhibit strong surface plasmon resonance along with a very high electromagnetic field, localized at its protrusions (Nehl et al. 2006; Kim et al. 2009). However, the existing methods for floral-shaped GNP synthesis involves the use of toxic chemical reagents and tedious multistep procedures (Wang et al. 2008) making the process hazardous and expensive.

Several physicochemical methods such as laser ablation, sonoelectrochemistry, photochemical and chemical reduction exist for GNP synthesis (Sylvestre et al. 2004; Serwas et al. 2008; Dong and Zhou 2007; Scampicchio et al. 2006). However, researchers are currently focusing on the biological route that utilizes an environmentally friendly solvent medium and a nontoxic material for stabilization. Biological systems have proved to be natural nano-factories leading to the production of stably-capped GNPs (Sharma et al. 2009). *Bacillus subtilis* was the first reported biological system for GNP synthesis (Beveridge and Murray 1980). Later, eukaryotes like fungi, algae and plant extracts were also found to effectively reduce gold ions to GNP (Soni and Prakash 2012; Luangpipat et al. 2011; Ghosh et al. 2012). Several fungi like *Aspergillus niger*, *Aspergillus nidulans*, *Penicillum* sp. and *Verticillium* sp. have also been used for GNP synthesis (Soni and Prakash 2012; Prusinkiewicz et al. 2012; Liangwei et al. 2011; Mukherjee et al. 2001). Fungi are greatly preferred for their capacity to secrete high amount of proteins, along with the advantage of easy handling, which make the downstream process simple (Sastry et al. 2003).

The current work describes the synthesis of extracellular floral-shaped GNP, by the reduction of gold ions using the aqueous extract of the fungus *Talaromyces flavus*. *Talaromyces flavus*, a novel fungal strain, has been reported to inhibit various soil-borne plant pathogens such as *Sclerotinia sclerotiorum*, *Rhizoctonia solani*, and *Verticillium dahlia.* (Boosalis 1956; Fravel et al. 1986; Mclaren et al. 1994). However, to the best of our knowledge, its potential to reduce gold ions to GNP has not yet been reported in the literature. This is the first report of a simple, green and rapid protocol for floral-shape GNP production using a fungal extract. The effect of different parameters required for the optimization of yield, controlled synthesis and minimization of the time for synthesis were studied.

Materials and methods

Fungal strain and its characterization

The fungal strain used in the study was isolated from a mine-contaminated site and subsequently maintained as pure culture on potato dextrose agar (HIMEDIA, India) slants. The strain was designated as IF3. Morphological characterization of the fungal strain was carried out by lactophenol cotton blue stain using a phase contrast microscope (Nikon H550L). Molecular characterization was done by 28S rDNA gene sequencing. DNA was isolated and the fragment of gene was amplified using the universal primers DF: 5'-ACCCCGCTGAACTTAAGC-3' and DR: 5'-GGTCCGTGTTTCAAGACGG-3'. The obtained sequence was then subjected to BLAST analysis and highly homologous gene sequences were selected and represented in the form of phylogenetic tree.

Biosynthesis of gold nanoparticles

A loopful of fungal spore was aseptically inoculated in 100 ml of sterile cornmeal medium (HIMEDIA) composed of cornmeal (20 g/l), peptic digest of animal tissue (10 g/l), yeast extract (4 g/l), and dextrose (10 g/l). The flasks were incubated at 35 °C for 72 h in an orbital shaker incubator at 150 rpm (Kuhner, Switzerland). The biomass obtained was filtered using Whatman filter paper and washed thoroughly with sterile distilled water to remove all media components. The washed biomass was further incubated in 100 ml of sterile distilled water under similar conditions for 72 h. Incubation in sterile distilled water subjects it to a stress condition, which allows the extracellular secretion of proteins and metabolites. The filtrate obtained after incubation was termed the extracellular fluid (ECF). In another set of experiment, ECF was boiled for 30 min and was termed the boiled extracellular fluid (BECF). In yet another set of experiment, the mycelia along with the ECF obtained after 72 h were boiled for 30 min. The resulting solution was filtered and termed the boiled biomass filtrate (BBF). All three filtrates were used for GNP production.

The ECF, BECF, and BBF were treated with chloroauric acid ($HAuCl_4$) and incubated for GNP synthesis. The concentration of $HAuCl_4$ was maintained at 1 mM, barring a few experiments. Three sets of control, comprising of cornmeal medium, ECF taken at 0 and 72 h of incubation were run simultaneously. The first two sets of the control were treated with 1 mM $HAuCl_4$ and the last set was run without $HAuCl_4$ addition.

The effect of ionic strength on the stability of GNP synthesized by biological and chemical method was studied by treating the synthesized GNP colloidal suspension with NaCl. Chemical synthesis of GNP was carried out using sodium citrate as the reducing agent (Turkevitch et al. 1951). The critical coagulation concentration (CCC) represents the NaCl concentration up to which the synthesized GNP remain stable without aggregation (Xie et al. 2003). In brief, CCC was determined by treating the synthesized GNP (biological and chemical) with gradual increasing concentration of NaCl, until a shift in the original SPR peak was observed. The stability with respect to the SPR band was established by recording the UV–visible absorbance of the mixture.

Characterization of the synthesized GNP and analysis of Extracellular fluid

Biosynthesis of GNP was visually observed by the change in color of the reaction mixture (ECF treated with $HAuCl_4$), and concordant production of GNP was confirmed using UV–vis Spectroscopic analysis (CECIL) in the range of 190–1,100 nm. Transmission electron microscopy (TEM) analysis of synthesized GNP was carried out to determine their size and shape. TEM microscope (FEI, TECNAI-G2) 20-TWIN operating at 200 kV equipped with a GATAN CCD camera was used for TEM-EDX analysis. The sample for TEM analysis was prepared by coating a drop of the colloidal gold solution onto a carbon-coated copper grid and allowing the solvent to evaporate under an IR lamp prior to analysis. To investigate the possible functional groups involved in GNP synthesis, Fourier transform infrared spectroscopy (FTIR, Perkin-Elmer Model Spectrum 1) analysis was carried out. The spectra were measured in the range of 4,000–400 cm^{-1} at a resolution of 2 cm^{-1}. A few drops of the sample were layered on top of a circular glass slide and allowed to dry, resulting in a thin film that was then analyzed. The crystalline nature and phase analysis of the synthesized GNP were studied using synchotron X-ray diffraction measurement. Diffraction pattern measurements were carried out on a Philips X'pert Pro, Panalytical X-ray powder diffractometer, having Cu-K α (λ=1.54 Å) radiation, working at 40 kV/30 mA. The X-ray patterns were obtained in the 2θ range of 10–79°, using 0.0050 step size. Dynamic light scattering (DLS) measurements were carried out to determine the hydrodynamic radius of synthesized GNP using a Dawn Heleos II (Wyatt) system operating at a wavelength of 658 nm.

All the three filtrates obtained (ECF, BECF, and BBF) were subjected to protein assay. Total protein content before and after GNP production was determined by the Folin-Lowry method (Lowry et al. 1951).

Result and discussion

Identification of the strain capable of GNP synthesis

The morphological and molecular identity of the fungus is depicted in Fig. 1. When grown on PDA plate, light yellow-colored mycelia with green spores and orange-yellow coloration were observed behind the plate (Fig. 1a). Figure 1b shows the morphological feature of the fungal strain as observed under a phase contrast microscope.

Molecular characterization of the fungal strain was done by 28S rDNA sequencing. The fragment of the D1/D2 region of the LSU (large subunit 28S rDNA) gene obtained from the isolated plasmid DNA was amplified by PCR. The inset in Fig. 1c shows the single discrete amplicon band of 650 bp when resolved on agarose gel. The consensus sequence of 611 bp of D2 region of the 28S rDNA gene generated was used to carry out BLAST. Based on the maximum identity score, the first ten sequences were selected and the phylogenetic tree was constructed using MEGA 4 software. On the basis of nucleotide homology and phylogenetic analysis (Fig. 1c), the isolate was identified to be *Talaromyces flavus* strain NRRL 2098 (GenBank Accession No.: EU021596.1).

Biosynthesis of gold nanoparticles using the fungal extracts and its kinetic analysis

On treating the ECF with $HAuCl_4$, a visible change in color from colorless to burgundy was observed within 24 h of incubation. Change in color of the solution indicated the bioreduction of chloroauric acid with the resultant formation of GNP. The formation of GNP was confirmed by UV–vis spectra with the appearance of a characteristic SPR peak in the range of 520–580 nm (Haiss et al. 2007). The control set comprising cornmeal medium showed GNP production indicating that the media components were also capable of reducing gold ions. However, the second set of control (ECF taken at 0 h of incubation) when treated with $HAuCl_4$ was not capable of GNP production, indicating complete washout of the medium components during biomass washing. The last set of the control (ECF obtained after 72 h of incubation without addition of $HAuCl_4$) did not show any change in color; however, when treated with $HAuCl_4$, it showed GNP production. The results thus clearly indicate that the fungal biomolecules secreted into the ECF during the 72 h of incubation were solely responsible for the reduction of the gold ions to GNP. Similarly, BECF and BBF were also treated with $HAuCl_4$, to study the role of denatured proteins on GNP synthesis. Interestingly, characteristic SPR peaks for GNP were obtained in both cases (Fig. 2). In addition, GNP synthesis in BBF was comparatively fast, i.e. within 5 h of $HAuCl_4$ addition. This rapid production may be due to the additional release of intracellular reducing components into the extract when subjected to boiling.

The kinetics of GNP biosynthesis was investigated to study the effect of reaction time on gold ion reduction. For this, aliquots of the reaction mixture were withdrawn at regular time intervals and scanned to obtain the absorption spectra. The evolution of optical density (OD) or absorbance at 540 nm for GNP synthesized using ECF and BECF is presented in Fig. 3a. It is apparent that, initially, GNP synthesis using ECF and BECF was slow, up to 120 and 240 min, respectively, after which the reaction was quite rapid for ECF, which showed a continuous increase in absorbance up to 24 h beyond which there was a slow increase. Comparatively, a slower pace of reaction was observed for BECF which showed a smaller but continuous formation of GNP even beyond 48 h. Even at 48 h of incubation, reaction is not

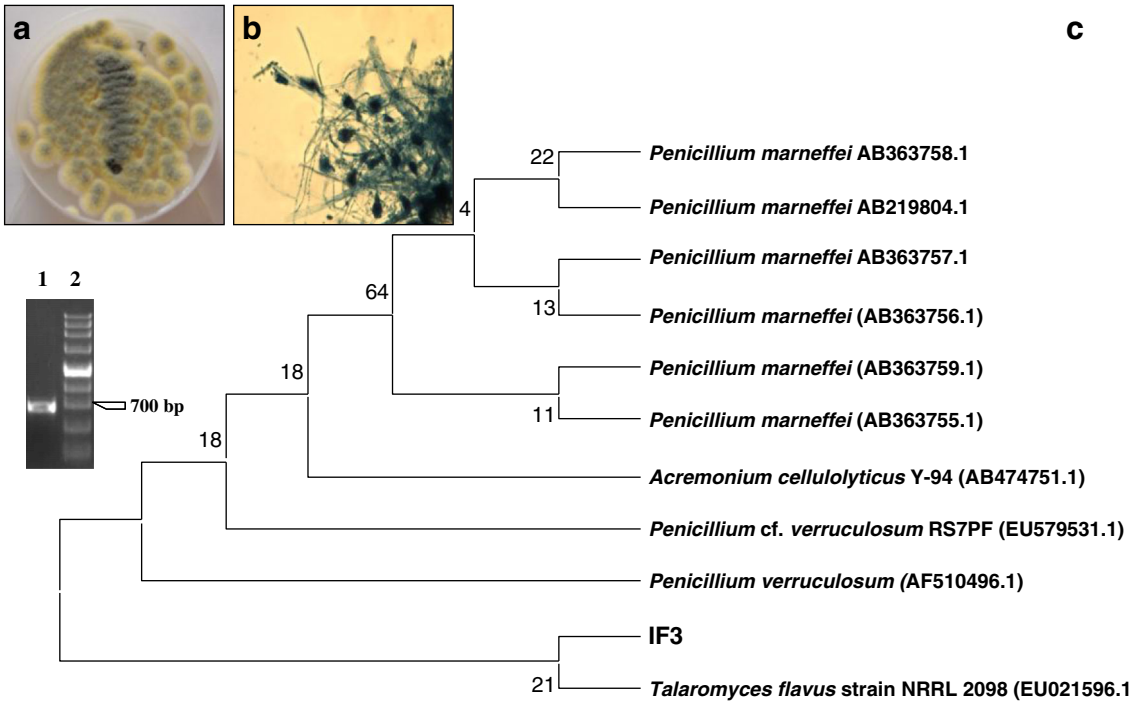

Fig. 1 **a**, **b** Morphological characteristics of *Talaromyces flavus*. **c** Phylogenetic tree depicting the evolutionary relationship of *Talaromyces flavus*. The *inset* in (**c**) shows the agarose gel image of PCR amplicon (*Lane 1* D1/D2 region of LSU (large subunit 28S rDNA) amplicon band; *lane 2* DNA marker)

complete as Au^{+} ions were still available for reduction. The reaction process may be slower because of less proteins/native proteins and/or reducing agent available in the BECF after boiling. Secondly, the obtained curves were sigmoidal in shape suggesting an autocatalytic reaction. An autocatalytic reaction involves a continuous but slow nucleation process followed by fast growth. For an autocatalytic reaction, the reaction rate is obtained by plotting ln[a/(1-a)] with respect to time (where a =OD(t)/OD(∞); OD(t) and OD(∞) are the O.D. at times t and ∞, respectively) and ln[a/(1-a)] is expected to change linearly with progressing time (Huang et al. 1993).

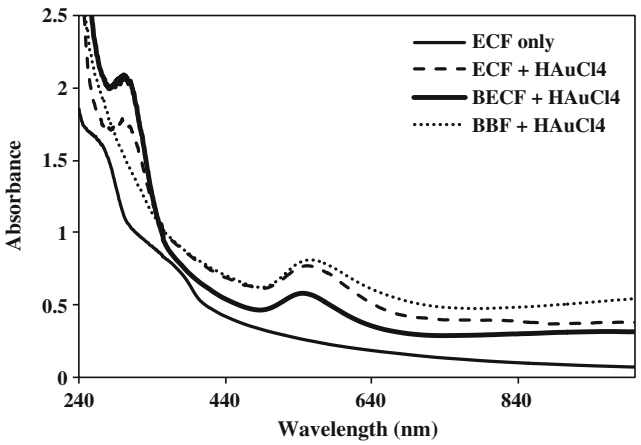

Fig. 2 UV–vis absorption spectra of GNP synthesized using boiled fungal extracts (condition: 1 mM $HAuCl_4$, 24 h)

The observed rate constant (k_{obs}) is obtained from the slope of the plot (Fig. 3b). The observed rate constant (k_{obs}) for ECF and BECF was found to be 0.032 and 0.014 h^{-1}, respectively.

Optimization of conditions for gold nanoparticle biosynthesis

The effect of initial concentration of gold salt ($HAuCl_4$) on GNP formation was studied by varying its concentration in the reaction mixture. Figure 4a shows the UV–vis spectra of GNP synthesized at different gold salt concentrations. At a low $HAuCl_4$ concentration of 0.5 mM, two distinct peaks at 535 and 740 nm was observed. The appearance of a peak in the longer wavelength region is because of longitudinal plasmon resonance implying the formation of anisotropic particles (Yu et al. 1997). With the gradual increase in gold salt concentration, a red shift in the transverse SPR peak was observed along with the complete disappearance of the longitudinal plasmon resonance peak. At 1 mM concentration, the SPR peak was observed at around 540 nm with the highest absorbance intensity. At a higher concentration of 1.5 and 2 mM, a broad SPR peak at around 555 nm was observed. This indicates that increasing the $HAuCl_4$ concentration beyond a certain limit leads to the formation of large and aggregated GNP. The obtained kinetic data showed that the observed rate constant was maximum for 1 mM concentration (k_{obs}=0.032 h^{-1}). The rate constant was found to increase with concentration, up to 1 mM $HAuCl_4$, and thereafter decreased with further increase

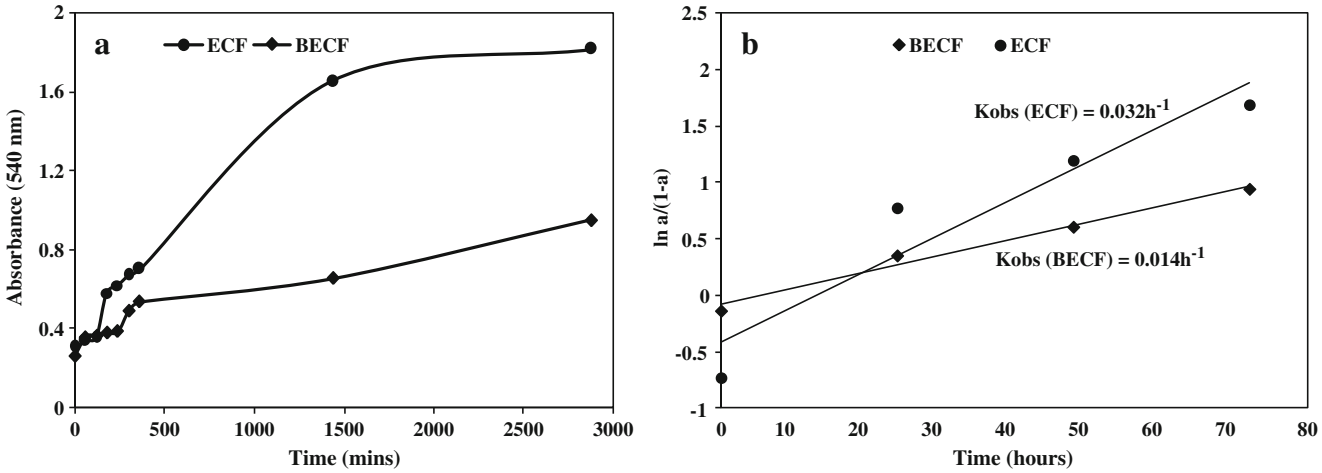

Fig. 3 **a** Evolution of absorbance intensity with time for GNP synthesized using ECF and BECF at 1 mM $HAuCl_4$ concentration. **b** Autocatalytic kinetic plot of resulting optical data of GNP synthesized using ECF and BECF

in concentration. The k_{obs} was 0.030, 0.032, 0.022, and 0.019 h^{-1} for 0.5, 1, 1.5, and 2 mM $HAuCl_4$ concentrations, respectively. Figure 4b illustrates the effect of initial concentration of $HAuCl_4$ on the observed rate constant. The result thus indicates that the reduction rate depends on the concentration of initial gold salt. As 1 mM $HAuCl_4$ concentration showed the maximum intensity of GNP production, it was consequently taken as the optimized concentration for further experiments.

The concentration of ECF was varied to study the effect of biomolecules on GNP biosynthesis. In brief, ECF was concentrated by lyophilization and treated in increasing concentrations (5, 10, 15, and 20 mg/ml) with 1 mM $HAuCl_4$. The UV–vis spectra presented in Fig. 5 reveals that, with the gradual increase in ECF concentration, the absorbance intensity of the synthesized GNP also increases, thereby confirming a direct relationship between the concentration of fungal biomolecules and GNP synthesis. A decrease in protein concentration in the reaction mixture was also observed after the formation of GNP (data not shown), which indicates the possible involvement of protein molecules as reducing or stabilizing agents in GNP synthesis. This study further proves that the components present in the fungal ECF carry out the bioreduction process and subsequent GNP production.

The influence of biomass amount on GNP production was studied by varying the sucrose concentration in the growth (cornmeal) medium. High concentrations of carbon source are known to enhance the growth of microorganisms leading to increased amounts of biomass, which in turn would enhance the secretion of biomolecules. As hypothesized, a gradual increase in sucrose concentration favored an increase in fungal biomass, resulting in higher protein content in the ECF (and may be other biomolecules responsible for GNP formation). Figure 6a presents the relationship between the sucrose concentration in the growth medium, the corresponding biomass weight, and protein concentration. At 2 % sucrose concentration, a sharp SRP peak was observed at 545 nm that signified

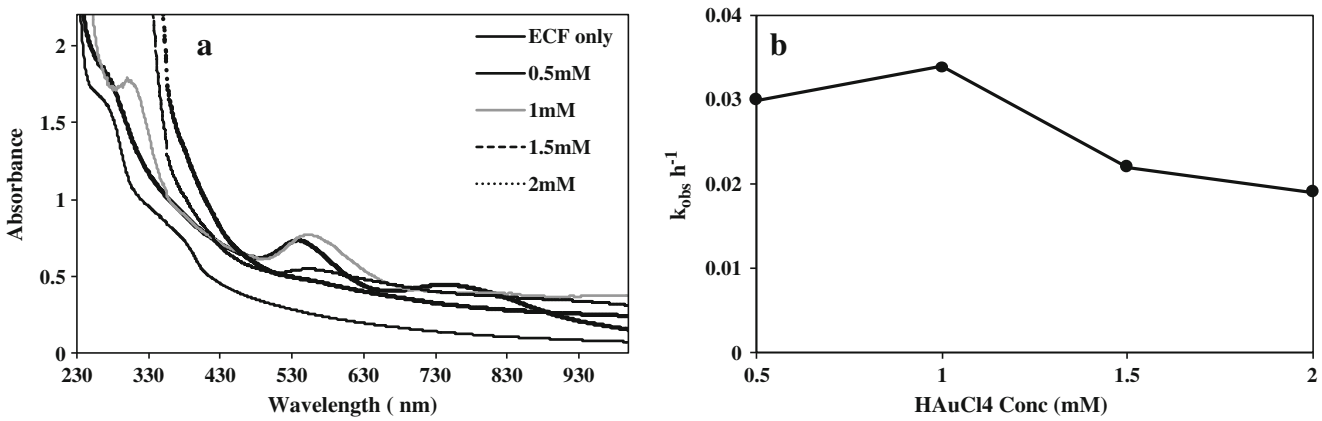

Fig. 4 **a** UV–vis absorption spectra of GNP synthesized at different concentrations of $HAuCl_4$ **b** The effect of initial concentration of $HAuCl_4$ on the observed rate constant

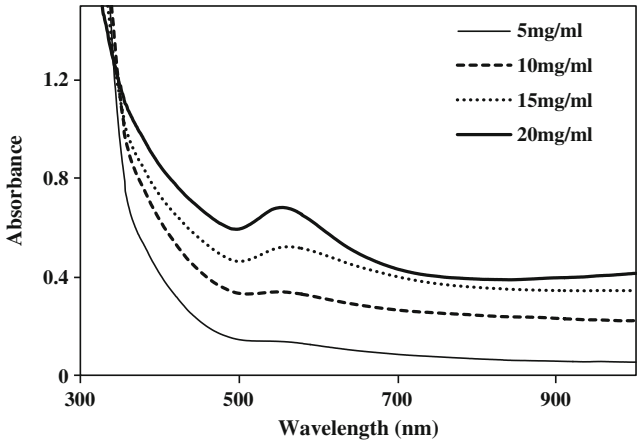

Fig. 5 UV–vis absorption spectra of GNP synthesized at different concentrations of ECF after 24 h of reaction

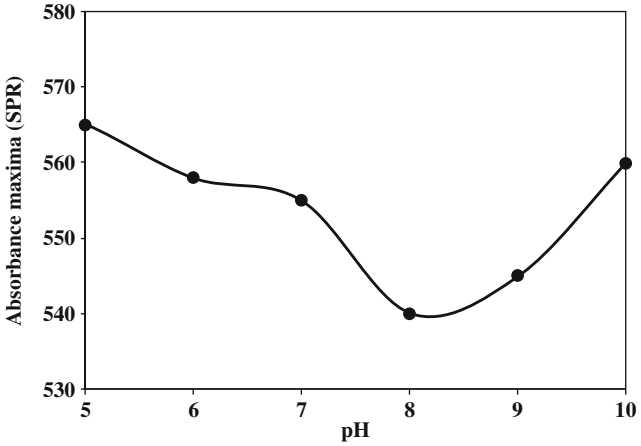

Fig. 7 Effect of initial pH of ECF on absorption maxima (SPR) of synthesized GNP

homogeneity and monodispersity of the synthesized nanoparticles. With a gradual increase in sucrose concentration, narrow peaks with enhanced intensity were observed. Even a decrease in reduction time was observed. With 5 % sucrose concentration, visible GNP production was observed within 3 h of treating the ECF with $HAuCl_4$. Increasing the sucrose concentration in media thus helps in a rapid reduction and enhanced GNP production. Figure 6b shows the absorbance intensity of synthesized GNP at different sucrose concentrations. Higher sucrose concentration led to high protein concentration which in turn resulted in enhanced GNP production. Thus, it can be inferred that proteins most likely play a role in the reduction and stabilization of GNP.

Literature survey emphasized that pH is yet another important factor in controlling the size of nanoparticles during their synthesis (Nayak et al. 2010). With this in mind, the effect of the pH of the reaction mixture on GNP production was investigated. The initial pH of fungal ECF was varied using dilute HCl and NaOH prior to $HAuCl_4$ addition, keeping other parameters constant. At different pH, the SPR peaks were centered at different wavelength maxima. GNP synthesized at inherent pH (pH 8) and pH 9 exhibited evident peaks at 540 nm. A peak with the maximum intensity was obtained at the inherent pH. However, with a decrease in the pH of the reaction mixture, the SPR peak shifted towards a longer wavelength and a decrease in intensity was also observed (Fig. 7). It has been reported that mostly amino, sulfydryl, and carboxylic acid groups are involved in nanoparticle formation. They are positively charged at low pH due to excessive protonation, altering the surface charge of the biomolecules and ultimately resulting in mild reduction and heterogeneity of the synthesized nanoparticles (Ahmad et al. 2002). Therefore, acidic pH triggers the formation of polydispersed nanoparticles. A gradual increase in pH leads to an increase in the reduction rate with controlled nucleation, and results in the formation of monodispersed and homogenous nanoparticles.

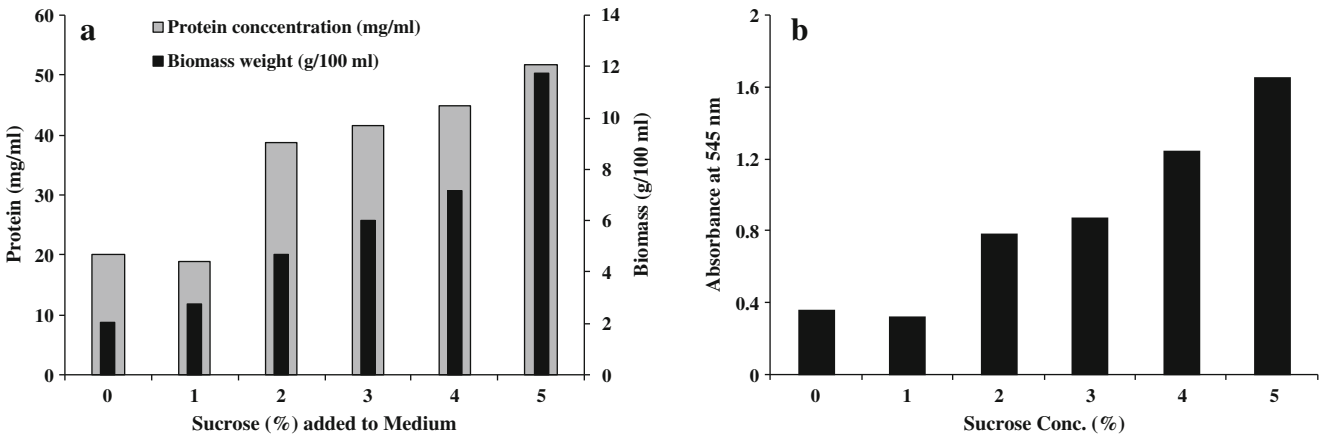

Fig. 6 **a** Effect of increasing sucrose concentration in the growth medium on biomass weight and protein concentration of ECF. **b** Effect of different sucrose concentration on absorbance intensity of synthesized GNP

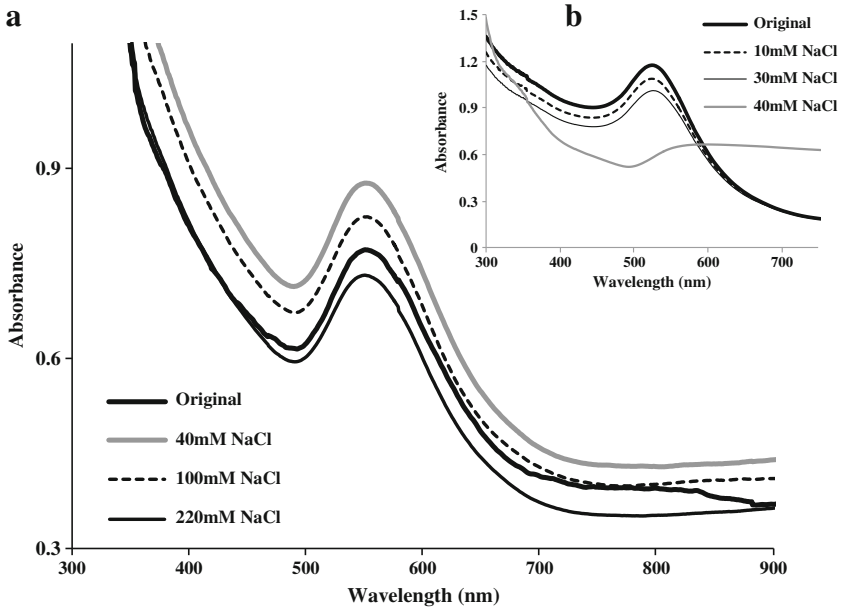

Fig. 8 UV–vis absorption spectra depicting the effect of ionic strength (NaCl concentration) on **a** biological and **b** chemically synthesized GNP

Effect of ionic strength on stability of biological and chemically synthesized GNP

Nanoparticles undergo coagulation at high salt (ionic strength) concentrations. Coagulation occurs due to the compression of the electrical double layer in the presence of high salt concentrations (Chandran et al. 2012). In the present study, it was observed that coagulation of chemically synthesized GNP occurred at much lower concentrations of NaCl compared to biological GNP. The biological GNP were stable up to 220 mM of NaCl concentration (Fig. 8a), whereas chemically synthesized GNP coagulated at 40 mM of NaCl (Fig. 8b). This suggests the high stability of biological GNP because of efficient capping that strongly shields the GNP, thereby resisting coagulation.

Characterization of synthesized gold nanoparticle

The exact phase composition and crystalline structure of the biosynthesized GNP were analyzed from the XRD diffractogram (Supplementary Fig. 1). The biosynthesized GNP were in an elemental form, Au^0, as established by the XRD analysis. The distinct Bragg reflection peaks at 2θ values of 38.0, 44.08, and 64.4 closely matched the standard XRD data for gold (JCPDS Card No: 00-001-1172) and corresponded to the crystal facets of (111), (200), and (220). The formed GNPs were consistent with the face-centered cubic (fcc) structure of gold, and thus synthesized GNP were undoubtedly crystalline in nature. An additional peak at 2θ value of 27.69 corresponding to that of AuCl was also observed (JCPDS Card No: 00-018-0568), depicting its existence as the dissolved precursor ion.

TEM images of GNP synthesized using ECF and BECF after 24 h confirms the metal particles to be in nanoscale, but were irregularly shaped and of varying size (Fig. 9a, b). The GNP formed using ECF were of floral shape. They possess a gold core surrounded by asymmetrical protrusions. Synthetic procedures undertaken for floral-shaped nanoparticle synthesis involves multiple steps and the use of hazardous chemicals, whereas, in the present case, floral-shaped GNP

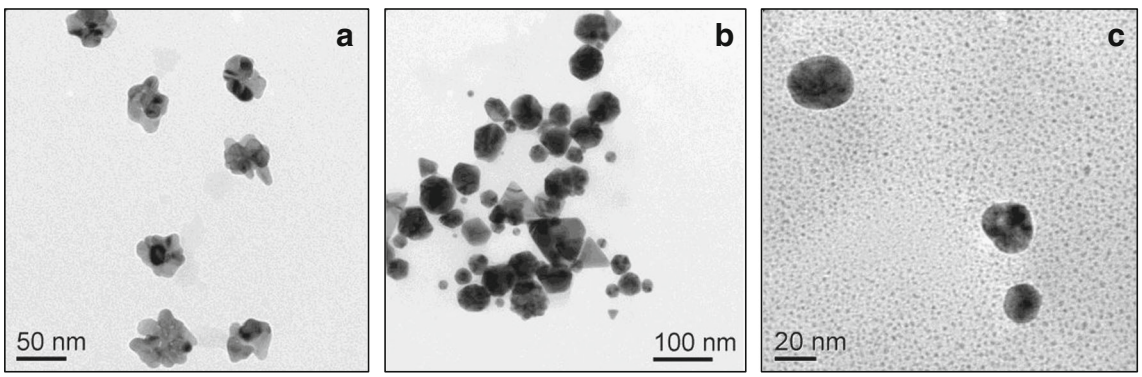

Fig. 9 Transmission electron micrographs of GNP synthesized using **a** ECF, **b** BECF, and **c** nucleation points of GNPs in ECF

synthesis involved a single step protocol and was rapid. Since floral-shaped nanoparticles are known to exhibit a high surface area and enhanced plasmon resonance, this single step biogenic synthesis of floral GNPs using *T. flavus* can be a major breakthrough in catalysis as well as biomedical applications. In the case of BECF, the synthesized GNP were polydispersed with a mixture of hexagonal, spherical, and triangular-shaped nanoparticles. Figure 9c shows the presence of some minute particles (even smaller than 1 nm) along with large particles. The former indicates the points of nucleation which fuse to form bigger particles.

Energy dispersive spectroscopic (EDS) analysis (Supplementary Fig. 2) showed the presence of strong signals corresponding to elemental gold along with signals for C, O, and Cu. Copper peaks were detected due to the use of copper grids in the TEM analysis, and the carbon and oxygen peaks are due the fungal biomolecules. The SAED image exhibits several diffraction ring patterns and further confirms the crystalline nature of the synthesized GNP. The particles were arranged in different planes which is in agreement with the XRD spectra.

The sizes of the GNP synthesized using ECF, BECF, and BBF were determined after 24 h by DLS analysis. GNP synthesized using BECF was comparatively of a very small size range with mean hydrodynamic radius (Rh) of 9.92±2.124 nm as compared to 38.54±10.347 and 40.92±5.682 nm in the case of ECF and BBF respectively (Supplementary Fig. 3). The obtained data are in good agreement with UV–vis spectra (Fig. 2) in which the SPR band of BECF is blue-shifted in comparison to those of ECF and BBF.

The comparison of FTIR spectra (Supplementary Fig. 4) of the fungal extract (ECF) before and after GNP synthesis was analyzed to identify the functional groups and biomolecules responsible for the reduction of Au^{+} ions and subsequent stabilization of the formed GNP. A board contour observed in the range of 3,600–3,200 cm^{-1} was the result of intermolecular hydrogen bonds formed between the –OH and $–NH_2$ groups of the protein molecules that broadens on formation of GNP, signifying the interaction of gold ions with the nitrogen atoms of the protein molecules (Sanghi and Verma 2010). Peaks at 3,063 cm^{-1} and 1,057 cm^{-1} in the GNP–fungal extract, corresponding to the =C-H stretch of alkene and the C-N stretch of aliphatic amines, respectively, indicate their presence in the extract. The N-H bending of amides results in the appearance of a peak at 1,543 cm^{-1} in the GNP–fungal extract. The disappearance of the peak at 1,254 cm^{-1} after the formation of GNP indicates the probable involvement of C-O groups. A shift in peak was observed from 744 to 785 cm^{-1} after GNP production, which was the result of out of plane N-H wagging of 1^{o} and 2^{o} amines. The disappearance of peaks at 543 cm^{-1} present in ECF after GNP formation indicates the involvement of S-S bonds (Silverstain and Webster 1998). Thus, FTIR spectra partially deciphered the involvement of –NH, –CO, and –SH groups as the possible capping agents.

Conclusion and future perspectives

In this paper, we report a rapid, ecofreindly, and feasible single step route for floral-shaped GNP biosynthesis using a novel fungal strain, *Talaromyces flavus.* The synthesized nanoparticles were of floral-shaped pattern with a mean hydrodynamic radius of 38.54±10.34. nm The bioreduction of gold ions to form GNP followed an autocatalytic reaction model, with an observed rate constant of 0.032 h^{-1}. A direct relationship between the concentration of fungal biomolecules and GNP biosynthesis was confirmed. FTIR analysis revealed the involvement of –NH, –CO, and –SH groups in the stabilization of synthesized GNPs. Thus, in addition to antimicrobial properties of the *Talaromyces flavus* extract, its capacity to synthesize floral-shaped GNPs is an additional breakthrough benefit in the fields of catalysis, SERS study, and biomedicines. However, the possible agents involved in the reduction and stabilization of GNP need further investigation. Studies concerning the mechanism and biochemistry of GNP synthesis can provide a complete knowledge on the molecular mechanism which can help control the size, shape, and monodispersity of nanoparticles.

Acknowledgment The authors would like to thank the reviewers for their valuable suggestions in improving the manuscript. E. Priyadarshini would like to express her sincere thanks to the Department of Science and Technology, New Delhi, India, for fellowship under the DST-Inspire Scheme.

References

Ahmad A, Mukherjee P, Mandal D, Senapati S, Khan MI, Kumar R, Sastry M (2002) Enzyme mediated extracellular synthesis of CdS nanoparticles by the fungus *Fusarium oxysporum*. Am Chem Soc 124:12108

Beveridge TJ, Murray RG (1980) Sites of metal deposition in the cell wall of Bacillus subtilis. J Bacteriol 141:876–87

Boca S, Rugina D, Pintea A, Barbu-Tudoran L, Astilean S (2011) Flower-shaped gold nanoparticles: synthesis, characterization and their application as SERS-active tags inside living cells. Nanotechnology 22: 055702 (7 pp)

Boosalis MG (1956) Effect of soil temperature and green-manure amendment of unsterilized soil on parasitism of *Rhizoctonia solani* by *Penicillium vermiculatum* and *Trichoderma* sp. Phytopathology 46: 473–478

Chandran PR, Naseer M, Udupa N, Sandhyarani N (2012) Size controlled synthesis of biocompatible gold nanoparticles and their activity in the oxidation of NADH. Nanotechnology 23:015602

Dong S, Zhou S (2007) Photochemical synthesis of colloidal gold nanoparticles. Mat Sci Eng B 140:153–159

Dykman L, Khlebtsov N (2012) Gold nanoparticles in biomedical applications: recent advances and perspectives. Chem Soc Rev 41:2256–2282. doi:10.1039/c1cs15166e

Eustis S, El-Sayed MA (2006) Why gold nanoparticles are more precious than pretty gold: Noble metal surface plasmon resonance and its enhancement of the radiative and nonradiative properties of nanocrystals of different shapes. Chem Soc Rev 35:209–217

Fravel DR, Davis JR, Sorenson LH (1986) Effect of *Talaromyces flavus* and metham on *Verticillum* wilt incidence and potato yield. Biol Cult Tests 1:17

Ghosh S, Patil S, Ahire M, Kitture R, Gurav DD, Jabgunde AM, Kale S, Pardesi K, Shinde V, Bellare J, Dhavale DD, Chopade BA (2012) Gnidia glauca flower extract mediated synthesis of gold nanoparticles and evaluation of its chemocatalytic potential. J Nanobiotechnol 10:17

Haiss W, Thanh NTK, Aveyard J, Fernig DG (2007) Determination of Size and Concnetration of Gold Nanoparticles from UV–vis Spectra. Anal Chem 79:4215–221

Hong X, Hall EAH (2012) Contribution of gold nanoparticles to the signal amplification in surface Plasmon resonance. Analyst 137: 4712–719. doi:10.1039/c2an35742a

Huang ZY, Mills G, Hajek B (1993) Spontaneous formation of Silver Particles in Basic 2-Propanaol J. Phys Chem 97:11542–11550

Huang J, Liu Z, Liu X, He C, Chow SY, Pan J (2005) Platinum nanoparticles from hydrosilylation reaction: capping agents, physical characterizations and electrochemical properties. Langmuir 21:699–704

Kim JH, Kang T, Yoo SM, Lee SY, Kim B, Choi YK (2009) A well-ordered flower-like gold nanostructure for integrated sensors via surface-enhanced Raman scattering. Nanotechnology 20:235302. doi:10.1088/0957-4484/20/23/235302

Liangwei D, Xian L, Feng J (2011) Rapid extra-/intracellular biosynthesis of gold nanoparticles by the fungus *Penicillium* sp. J Nanopart Res 13:921–930. doi:10.1007/s11051-010-0165-2

Lowry OH, Rosenbrough NJ, Farr AL, Randall RJ (1951) Protein measurement with the Folin-Phenol reagents. J Biol Chem 193:265–275

Luangpipat T, Beattie IR, Chisti Y, Haverkamp RG (2011) Gold nanoparticles produced in a microalga. J Nanopart Res. doi:10.1007/s11051-011-0397-9

Mclaren DL, Huang HC, Kozub GC, Rimmer SR (1994) Biological control of sclerotinia wilt of sunflower with *Talaromyces flavus* and *Coniothyrium minitans*. Plant Dis 78:231–235

Mukherjee P et al (2001) Bioreduction of $AuCl_4^-$Ions by the Fungus, *Verticillium* sp. and surface trapping of the gold nanoparticles formed. Angew Chem Int Ed 40:3585–3588

Nayak RR, Pradhan N, Behera D, Pradhan KM, Mishra S, Sukla LB, Mishra BK (2010) Green synthesis of silver nanoparticle by Penicillium purpurogenum NPMF: the process and optimization. J Nanopart Res. doi:10.1007/s11051-010-0208-8

Nehl LH, Liao H, Hafner JH (2006) Synthesis and Optical properties of Star- shaped gold nanoparticles. Nano Lett 6:683. doi:10.1021/nl052409y

Prusinkiewicz MA, Farazkhorasani F, Dynes JJ, Wang J, Gough KM, Kaminskyj SGW (2012) Proof-of-principle for SERS imaging of *Aspergillus nidulans* hyphae using in vivo synthesis of gold nanoparticles. Analyst. doi:10.1039/c2an35620a

Sanghi R, Verma P (2010) pH dependent fungal proteins in the green synthesis of gold nanoparticles. Adv Mat Lett 1(3):193–199. doi:10.5185/amlett.2010.5124

Sardar R, Funston AM, Mulvaney P, Murray RW (2009) Gold nanoparticle: past, present and future. Langmuir 25(24):13840–51. doi:10.1021/la9019475

Sastry M, Ahmad A, Khan MI, Kumar R (2003) Biosynthesis of metal nanoparticles using fungi and actinomycete. Curr Sci 85:162–170

Scampicchio M, Wang J, Blasco AJ, Arribas AS, Mannino S, Escarpa A (2006) Nanoparticle-based assays of antioxidant activity. Anal Chem 78:2060–2063

Schmid G, Simon U (2005) Gold nanoparticles: assembly and electrical properties in 1–3 dimensions. Chem Commun,p 697–710. doi:10.1039/b411696h

Serwas AH, Delplancke JL, Jerome R, Jerome C, Canet L (2008) Preparation of stable suspensions of gold nanoparticles in water by sonoelectrochemistry. Ultrason Sonochem 15:1055–1061

Sharma VK, Yngard RA, Lin Y (2009) Silver nanoparticles: green synthesis and their antimicrobial activities. Adv Colloid Interface Sci 145:83–96. doi:10.1016/j.cis.2008.09.002

Silverstain RM, Webster FX (1998) Spectrometric identification of organic compounds, 6th edn. Wiley, New York, pp 71–143

Soni N, Prakash S (2012) Synthesis of gold nanoparticles by the fungus *Aspergillus niger* and its efficacy against mosquito larvae. Rep Parasitol 2:1–7. doi:10.2147/RIP.S29033

Stratakis M, Garcia H (2012) Catalysis by supported gold nanoparticles: beyond aerobic oxidative processes. Chem Rev 112:446–4506. doi:10.1021/cr3000785

Sylvestre JP, Kabashin AV, Sacher E, Meunier M, Luong JHT (2004) Stabilization and size control of gold nanoparticles during laser ablation in aqueous cyclodextrins. J Am Chem Soc 126:7176–7177

Turkevitch J, Stevenson PC, Hiller J (1951) Nucleation and growth process in the synthesis of colloidal gold. Discuss Faraday Soc 11: 55–75

Wang L, Wei G, Guo C, Sun L, Sun Y, Song Y, Yang T, Li Z (2008) Photochemical synthesis and self assembly of gold nanoparticles. Colloids Surf A 312:148–153. doi:10.1016/j.colsurfa.2007.06.043

Xie H, Tkachenko AG, Glomm WR, Ryan JA, Brennaman MK, Papanikolas JM, Franzen S, Feldheim DL (2003) Critical flocculation concentrations, binding isotherms, and ligand exchange properties of peptide-modified gold nanoparticles studied by UV–Visible, fluorescence, and time-correlated single photon counting spectroscopies. Anal Chem 75:5797–805

Yu Y, Chnag SS, Lee CL, Wang CRC (1997) Gold nanorods: elecrochemical synthesis and optical properties. J Phys Chem B 101:6661. doi:10.1021/jp971656q